

The Mechanism of SEI Formation on a Single Crystal Si(100) Electrode

Ulrike S. Vogl,^{a,b} Simon F. Lux,^{b,*} Ethan J. Crumlin,^c Zhi Liu,^c Lydia Terborg,^b Martin Winter,^{a,**,z} and Robert Kostecki^{b,*,z}

^aWestfälische Wilhelms-Universität Münster, MEET Battery Research Centre, Institute of Physical Chemistry, 48149 Münster, Germany

^b Environmental Energy Technologies Division, Lawrence Berkeley National Laboratory, Berkeley, California 94720, USA

^cAdvanced Light Source, Lawrence Berkeley National Laboratory, University of California, Berkeley, California 94720, USA

A fundamental study of interfacial phenomena on a Si(100) single crystal electrode in organic carbonate-based electrolytes was carried out. The SEI formation on the Si(100) single crystal electrode was investigated as a function of the electrolyte composition, electrode potential and Li_xSi lithiation degree. Fourier transform infrared spectroscopy (FTIR) and X-ray photon spectroscopy (XPS) studies of the SEI layer during early stages of SEI formation indicate a strong dependence of the SEI composition on the electrolyte composition. However, the influence of the electrolyte composition becomes negligible at low potentials, when lithium alloys with Si and forms amorphous Li_xSi . The effect of vinylene carbonate (VC) and fluoroethylene carbonate (FEC) electrolyte additives on the composition of the SEI layer was evaluated.

© The Author(s) 2015. Published by ECS. This is an open access article distributed under the terms of the Creative Commons Attribution 4.0 License (CC BY, http://creativecommons.org/licenses/by/4.0/), which permits unrestricted reuse of the work in any medium, provided the original work is properly cited. [DOI: 10.1149/2.0391504jes] All rights reserved.

Manuscript submitted November 3, 2014; revised manuscript received January 12, 2015. Published January 22, 2015.

Currently, graphite is the most common negative electrode material in commercial lithium ion batteries for portable electronics. $^{1-3}$ However, lithium ion batteries for large-scale transportation applications require new inexpensive electrode materials with higher specific capacity. For decades, silicon has been considered as a promising negative electrode material, mainly because of its high specific capacity of ca. 3500 mAh/g 4 and its abundance in the earth crust. $^{4-6}$ The key problems that prevent its widespread use are large, up to $\sim\!300\,\%$ volumetric changes during lithiation/delithiation processes and interfacial instability of lithium silicides in organic solvent based electrolytes. $^{6-12}$ The resultant poor electrochemical cycling performance and large irreversible capacities during formation and operation of the Si negative electrode contribute to rapid degradation and failure of the battery. $^{6.7,13}$

The solid electrolyte interphase (SEI) layer, which forms at the electrode/electrolyte interface during the initial charge/discharge cycles, is the key component that determines the long-term stability and cycling behavior of carbonaceous and intermetallic negative Li-ion battery electrodes. ^{14–16} Electrolyte reduction and SEI layer formation on a Si electrode usually take place at potentials below 1.8 V vs. Li/Li⁺ and accompany the formation of Li-Si phases, the so-called "Si-Li alloying" process at E <0.4 V vs. Li/Li⁺. ¹⁷ The exact mechanism of the SEI formation processes on Si, the SEI composition and the effect on the Si electrode electrochemical cycling performance is not well understood. ¹⁸ On the other hand, SEI-forming electrolyte additives such as vinylene carbonate (VC) and fluoroethylene carbonate (FEC) are known to alter the composition and properties of the SEI on Si and improve the electrode electrochemical performance. ^{19–21}

Interestingly, recent model studies on Sn single crystal electrodes in organic carbonate electrolytes revealed a strong correlation between the crystal surface orientation and the SEI composition. ^{22,23} A similar study of the composition of the SEI on a silicon monocrystal electrode showed strong effects of different SEI formation protocols, presence/absence of intrinsic SiO₂, electrolyte composition and impurities e.g., HF.^{24–26} Also graphite exhibits different SEI layer compositions on plane and edge sites. ^{18,27,28} In this study, the mechanism of SEI formation on a model binder- and conductive additive-free Si(100) wafer electrode is studied as a function of the electrode potential and electrolyte composition.

Experimental

Commercial single crystal Si(100), n-type (\sim 10 Ω ·cm resistivity), 500 µm thick wafers were obtained from Silicon Quest International (San Jose, USA). The wafers were cut into 1×1 cm pieces and heated at 195°C under vacuum for 48 h to remove adsorbed water.²⁹ The baseline electrolyte 1M LiPF₆, EC:DEC [3:7 wt] was prepared by dissolving lithium hexafluorophosphate (LiPF₆) (Sigma Aldrich, battery grade) in a mixture of ethylene carbonate (EC) and diethylene carbonate (DEC) (Sigma Aldrich, battery grade). Fluoroethylene carbonate (FEC) (Solvay S.A., battery grade) and vinylene carbonate (VC, Sigma Aldrich, battery grade) additives were used to prepare 1 M LiPF₆, FEC:EC:DEC [10:27:63] and 1M LiPF₆, VC:EC:DEC [2:29.4:68.6] electrolytes. Electrochemical experiments were carried out in a three-electrode test cell with Li-foil counter and reference electrodes (Figure 1), using a Reference 600 Potentiostat/Galvanostat/ZRA (Gamry Instruments). Linear sweep voltammetry scans were performed at a 0.025 mV/s scan rate. Prior to spectroscopic and microscopic measurements, the Si(100) electrodes were removed from the electrochemical cell, soaked in DEC three times and dried under vacuum for 5 min. All materials and sample handling were conducted in a He-filled glove box (VAC Nexus one, O2 and $H_2O < 1$ ppm). All potentials are referred vs. the Li/Li⁺ electrode.

Transmission FTIR spectra were recorded in a N_2 -filled environmental chamber using a MB102 (Bomem) spectrometer equipped with CsI windows. The Si electrodes were transferred from the glove

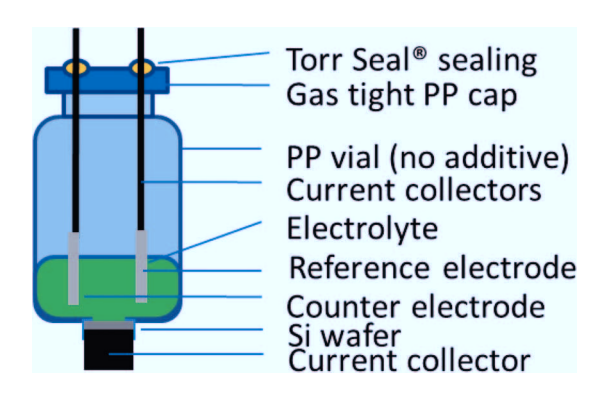


Figure 1. Schematic diagram of the three-electrode test cell.

^{*}Electrochemical Society Active Member.

^{**}Electrochemical Society Fellow.

^zE-mail: r_kostecki@lbl.gov; martin.winter@uni-muenster.de

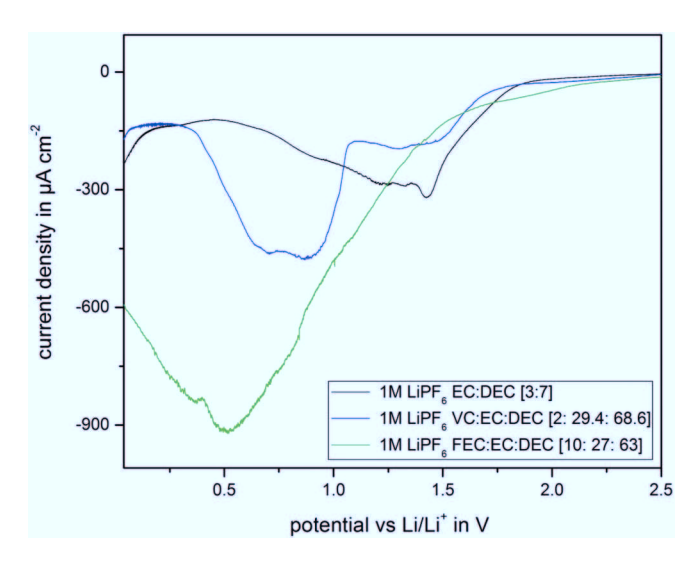


Figure 2. Linear sweep voltammograms of the Si(100) electrode in 1M LiPF₆, EC:DEC [3:7], 1M LiPF₆, VC:EC:DEC [2:29.4:68.6], and 1M LiPF₆, FEC:EC:DEC [10: 27:63].

box to the environmental chamber in a sealed airtight container. All FTIR spectra were baseline corrected for the pristine silicon wafer. Scanning electron micrographic (SEM) images were collected in a Zeiss Gemini Ultra Field-Emission Scanning Electron Microscope (Peabody, USA) equipped with an energy dispersive X-ray spectrometer (Thermo Electron).

X-ray photon spectroscopy (XPS) measurements were performed at the Advanced Light Source (ALS) beamline 9.3.1 in the Lawrence Berkeley National Laboratory (LBNL). All XPS spectra, survey (-5 to 950 eV), C 1s, F 1s, P 2p, O 1s, Li 1s, Si 2p, Cl 2p were collected at the photon energy of 4 keV. The spectra were calibrated to the C 1s photoemission peak of adventitious hydrocarbons at 285.0 eV. A spectral analysis of the photoemission bands was done after subtracting a Shirley-type background using a symmetric Gaussian-Lorentzian function. The Si 2p and P 2p peak doublets were treated by a fixed energy separation of 0.6 eV and 1.2 eV, respectively and at a branching ratio of 0.5.

Results and Discussion

Figure 2 depicts linear sweep voltammetric profiles of the Si (100) electrode in 1M LiPF₆, EC:DEC [3:7], 1M LiPF₆, VC:EC:DEC [2:29.4:68.6] and 1M LiPF₆, FEC:EC:DEC [10:27:63] electrolytes. The cathodic current threshold, the current peaks potentials and the total charge consumed (Table I) vary significantly with the electrolyte composition, which may indicate different interfacial reaction pathways and rates. The current response in the 1M LiPF₆, EC:DEC [3:7] baseline electrolyte shows a peak at 1.5 V followed by a broad and featureless current tail. In the presence of FEC the current shows a broad maximum at \sim 0.5 V, whereas the VC-containing electrolyte displays two strong cathodic peaks at 0.8 and 0.6 V and a broad shoulder

Table I. Current-charge characteristics of cathodic linear sweep voltammograms (Figure 2) of the Si(100) electrode in 1M LiPF₆, EC:DEC [3:7], 1M LiPF₆, VC:EC:DEC [2:29.4:68.6] and 1M LiPF₆, FEC:EC:DEC [10:27:63].

Electrolyte	1M LiPF ₆ , EC:DEC [3:7]	1M LiPF ₆ , VC:EC:DEC [2:29.4:68.6]	1M LiPF ₆ , FEC:EC:DEC [10:27:63]
Peak current density (μA cm ⁻²)	330 (at 1.4 V)	480 (at 0.9 V)	920 (at 0.5 V)
Total consumed charge (C)	4.38	5.52	11.88
On-set potential of electrolyte decomposition (V)	1.8	1.6	2.1

centered around 1.3 V similar to the current features observed in the baseline electrolyte. The on-set potential of electrolyte decomposition in the baseline electrolyte is located at 1.8 V, which is consistent with literature. ¹⁷ It is shifted by 0.2 V to lower potentials in the presence of VC, but in the 1M LiPF₆, FEC:EC:DEC [10:27:63] electrolyte it is observed at higher potentials, at ca. 2.1 V (Table I). The total charge consumed by the electrolyte reduction reactions during the initial potential scans increases slightly in the presence of VC but nearly triples in 1 M LiPF₆, FEC:EC:DEC [10:27:63].

The presence of VC and FEC induces different SEI formation pathways at different potentials (Figure 2), which usually results in an improvement of the cycling performance of Si in lithium ion batteries. ^{20,21,30} To unveil processes, which occur during the early stages of SEI formation, two series of control experiments were carried out. One set of electrode samples was obtained from electrochemical experiments on an unlithiated Si(100), where the linear voltammetric scan was stopped at 0.5 V i.e., before the Li-Si alloying. ¹⁷ The other set of electrodes was removed from the cell after scanning the potential to 0.01 V, i.e., when the surface of the Si wafer electrode becomes fully lithiated and amorphous Li_xSi. ^{6,8}

SEM images of the Si(100) electrodes removed at 0.5 V are shown in Figure 3. The morphology of the SEI layer formed in the additive-free baseline electrolyte is rough, highly inhomogeneous and consists of particles and agglomerates of various sizes. The SEI layers obtained in the VC- and FEC-containing electrolytes appear more uniform and homogeneous. The elongated cracks and channels observed in Figure 3b most likely originate from the drying process prior to the SEM investigation.

EDX elemental analysis of the surface films (Table II) shows signals for carbon, oxygen, fluorine, phosphorus and silicon. The Si background signal doubles for the electrode from the VC-containing electrolyte and it becomes huge for the electrode stemming from the FEC-containing electrolyte. The intensity of the silicon signal from the Si(100) substrate depends on the SEI composition and is proportional to the thickness of the SEI, which presents a quite opposite trend to the observed pattern of consumed cathodic charge (Table I), assuming that more charge results in a thicker SEI, which should screen better the Si substrate. This may indicate that the majority of the reduction products formed in the 1M LiPF₆, VC:EC:DEC [2:29.4:68.6] and 1 M

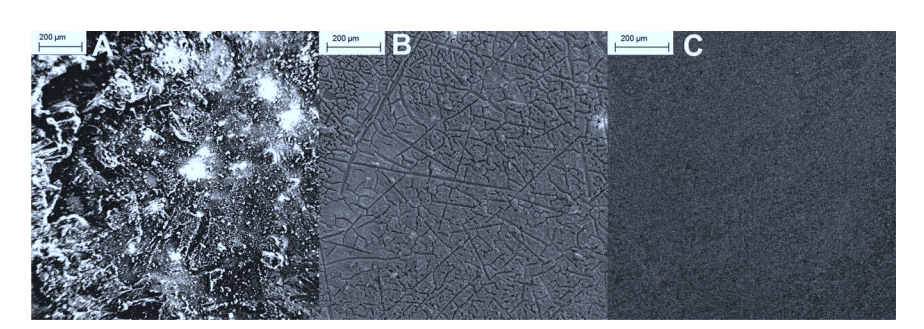


Figure 3. SEM images of the Si(100) electrode removed at a potential of 0.5 V from 1M LiPF₆, EC:DEC [3:7] (A), 1M LiPF₆, VC:EC:DEC [2:29.4 68.6] (B) and 1M LiPF₆, FEC:EC:DEC [10:27:63] (C).

Table II. Relative elemental composition of the SEI on Si(100) at 0.5 V in 1M LiPF₆, EC:DEC [3:7], 1M LiPF₆, VC:EC:DEC [2:29.4:68.6] and 1M LiPF₆, FEC:EC:DEC [10:27:63].

Electrolyte	C	O	F	Si	P [%]
1M LiPF ₆ , EC:DEC [3:7]		16.00			
1M LiPF ₆ , VC:EC:DEC [2:29.4:68.6]					
1M LiPF ₆ , FEC:EC:DEC [10:27:63]	28.43	06.70	18.10	46.60	00.18

LiPF₆, FEC:EC:DEC [10:27:63] electrolytes are soluble and diffuse away in the electrolyte immediately after formation. Another possibility is that the deposition mechanism of the electrolyte with FEC follows multi-electron pathways and thus more charge is consumed per solvent/salt molecule.

Figure 4 shows FTIR spectra for the SEI layers formed at 0.5 V in the three electrolytes. The spectra display different characteristics clearly indicating variations of chemical composition in the corresponding SEI layers. Similarly to the studies of Tsubouchi et al.³¹ and Profatilova et al.,32 the FTIR spectra consist of features associated with each electrolyte component. LiPF₆ decomposition products appear as a broad peak at 500 cm⁻¹ for $v_{\text{(Li-F)}}$ in LiF, a peak at 842 cm⁻¹ for $v_{(P-F)}$ in PF₃, and peaks at 982, 905 and 730 cm⁻¹ represent the the $\nu_{\text{(P-O-C)}}$ stretching modes in P(OR)₃. The triplet at $1775~\text{cm}^{-1}$ corresponds to the $\nu_{(C=O)}$ stretch modes of DEC and EC decomposition products.³² The asymmetric stretching mode $v_{(C=O)}$ at 1484 cm⁻¹ can be attributed to decomposition products of EC whereas the symmetric mode $v_{(C=0)}$ at 1300 cm⁻¹ originates from products of DEC reduction. The two peaks at 1200 and 1086 cm⁻¹ are characteristic for carbonate ring stretching modes $v_{(C-O)}$ of EC decomposition products. The peak at 1410 cm⁻¹ is attributed to bending modes of the CH₃/CH₂/CH groups. The FTIR spectrum of the SEI layer formed at 0.5 V vs. Li/Li⁺ in 1M LiPF₆ in VC:EC:DEC [2:29.4:68.6] shows similar bands at 1200 and 1086 cm⁻¹ of the EC decomposition products and a strong band from LiF at 500 cm⁻¹ in comparison to the baseline electrolyte.

The FTIR spectrum of the SEI layer grown in the presence of FEC is somewhat similar to the spectrum of the SEI formed in the baseline electrolyte. The peak distribution pattern between 600 and $1500\,\mathrm{cm^{-1}}$ is comparable to the spectrum from the baseline electrolyte. However, the $\nu_{(Li\text{-}F)}$ peak at $500\,\mathrm{cm^{-1}}$ and bands representing the DEC decomposition products at 1300 and $1775\,\mathrm{cm^{-1}}$ appear to be more intense in relation to the other bands. The additional broad

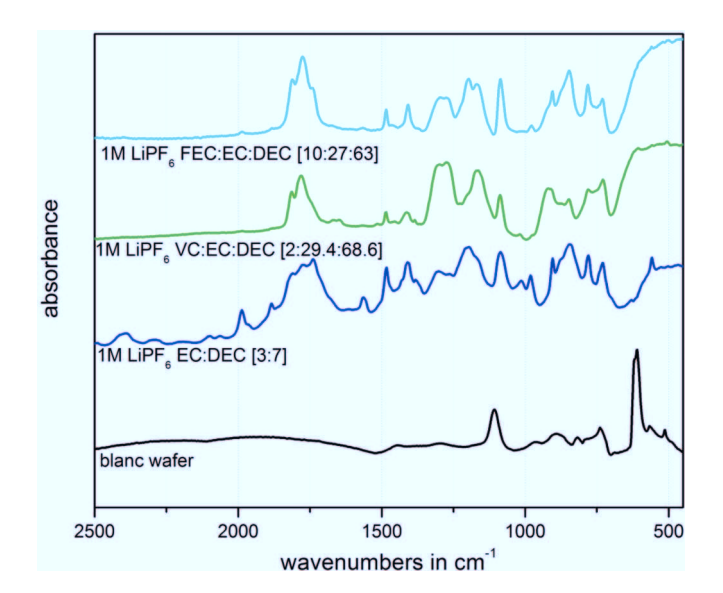


Figure 4. Ex situ FTIR spectra of the Si(100) electrode removed at 0.5 V from 1M LiPF₆, EC:DEC [3:7], 1M LiPF₆, VC:EC:DEC [2:29.4:68.6] and 1M LiPF₆, FEC:EC:DEC [10:27:63].

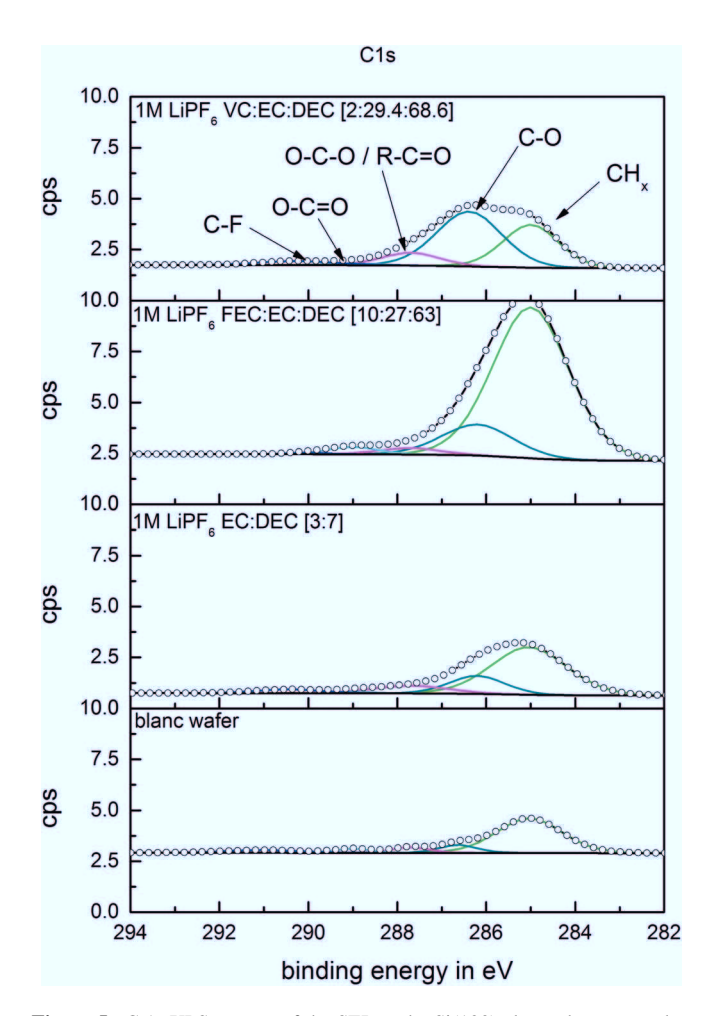


Figure 5. C 1s XPS spectra of the SEI on the Si(100) electrodes removed at 0.5 V from 1M LiPF₆, EC:DEC [3:7], 1M LiPF₆, VC:EC:DEC [2:29.4:68.6] and 1M LiPF₆, FEC:EC:DEC [10:27:63].

spectral features at 1980 and 1860 cm⁻¹ may indicate a wider variety of decomposition products at the Si(100) electrode in the baseline electrolyte. The FTIR spectrum of the Si(100) electrode in the VC-containing electrolyte shows a radically different peak distribution pattern. Especially, the high profile of the peaks at 1300 cm⁻¹ and in between 500 and 1000 cm⁻¹ deviates from the observed spectra of the Si(100) electrode in the baseline and FEC-containing electrolytes.

Figure 5 shows C 1s XPS spectra of the SEI layers on Si(100) electrode formed during the linear voltammetric scan to 0.5 V. The spectra are dominated by the C-H bond at 285.0 eV, C-O bond at 286.3 eV, O-C-O/R-C=O bonds at 287.7 eV and C=O bonds from ketones/esters at 289 eV. 25,33,34 The relative C-H/C-O band intensities vary significantly between the samples and are the highest for the SEI from the FEC-containing electrolyte and the lowest for the VC-containing electrolyte. The VC-containing electrolyte appears to favor formation of SEI compounds with C-O and O-C-O functional groups, possibly originating from VC polymerization products. ^{19–21,35}

The corresponding F 1s XPS spectra in Figure 6 show a Li-F peak at 685.9 eV, ^{17,25,33,34} SiOF peak at 687.4 eV and traces of C-F and LiPF₆ at 689.0 and 689.7 eV, respectively. ¹⁷ The spectrum of the SEI formed at 0.5 V in the VC-containing electrolyte is dominated by the signal from SiOF, whereas LiF is the main component of the spectra for the baseline and FEC-containing electrolytes. Traces of C-F species and LiPF₆ residues can be found in all spectra.

The Si 2p spectrum of the SEI formed in the baseline electrolyte is almost completely featureless (Figure 7), including a total lack of signals from the bulk Si substrate. The Si 2p spectra of the Si(100) electrode from the FEC-containing electrolyte display contributions

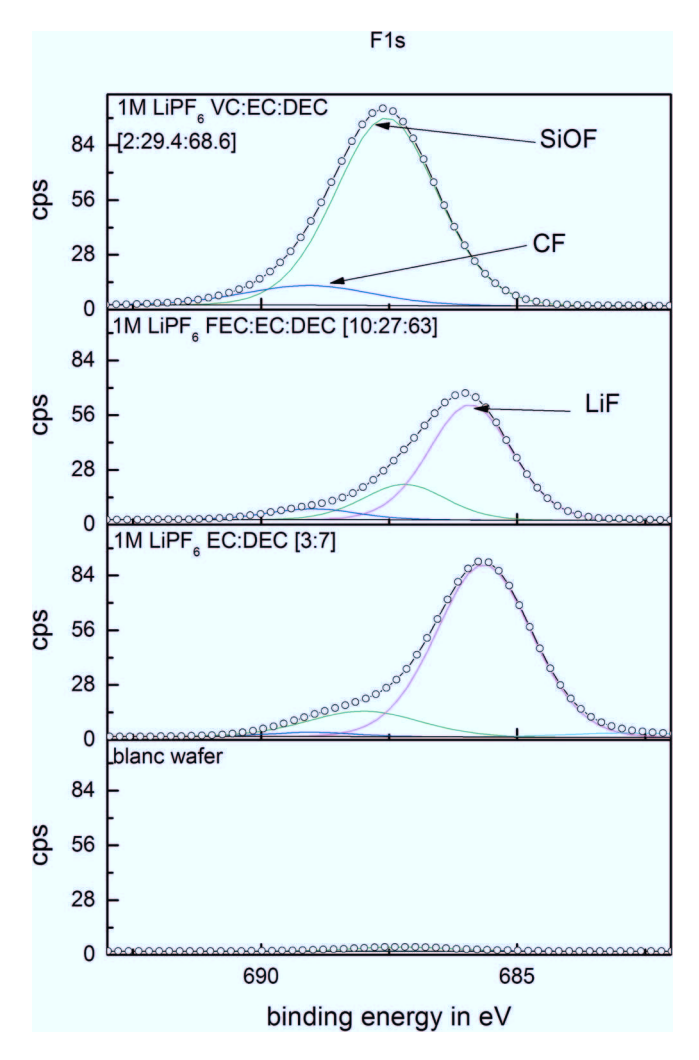


Figure 6. F 1s XPS spectra of SEI on the Si(100) removed at 0.5 V from 1M LiPF₆, EC:DEC [3:7], 1M LiPF₆, VC:EC:DEC [2:29.4:68.6] and 1M LiPF₆, FEC:EC:DEC [10:27:63].

from the bulk silicon at 99.1 and 99.6 eV. 25,33,34,36 Additionally, peaks of Li_xSi at 98.4 eV and 98.9 eV are clearly identifiable. 25,33,34,36 The presence of Li-Si bonds is not attributed to a Li-Si alloying reaction because it happens at potentials above 0.5 V. 17 However, the intrinsic SiO₂ layer on Si(100) reacts with Li⁺, resulting in a partial conversion of the surface oxide to Li₂O and lithium silicates Li₂Si₂O₅ at 0.5 V. $^{37-40}$ The presence of SiOF in the samples from FEC- and VC-containing electrolytes as indicated by the signals at 105.1 and 105.6 eV, is fully consistent with the corresponding F 1s XPS spectra (Figure 6). 33,34,36 The Si-O peaks from SiO₂ at 103.6 and 104.2 eV^{19,33,34,36} and a small amount of lithium silicates at 101.0 and 101.6 eV^{33,34,36} can also be observed. The SEI from the VC-containing electrolyte also shows the highest relative signal of the bulk Si material which may indicate a thin and/or porous SEI film.

The EDX, FTIR and XPS analysis of the SEI layers formed at E>0.5 V in these electrolytes points at significant variations of chemical composition, which are consistent with the observed differences in the voltammetric profiles, film thickness and morphology.

To further explore the evolution of the SEI on the Si(100) electrode upon Li-Si alloying, the linear voltammetric scans were extended to 0.01 V i.e., to a potential, where the surface of the silicon wafer becomes fully lithiated. The SEM pictures of all SEI layers at 0.01 V look very similar (not shown here) and show no distinguishable morphology features. The FTIR spectra of the Si(100) electrode scanned to 0.01 V in the tested electrolytes (Figure 8) reveal only minor dif-

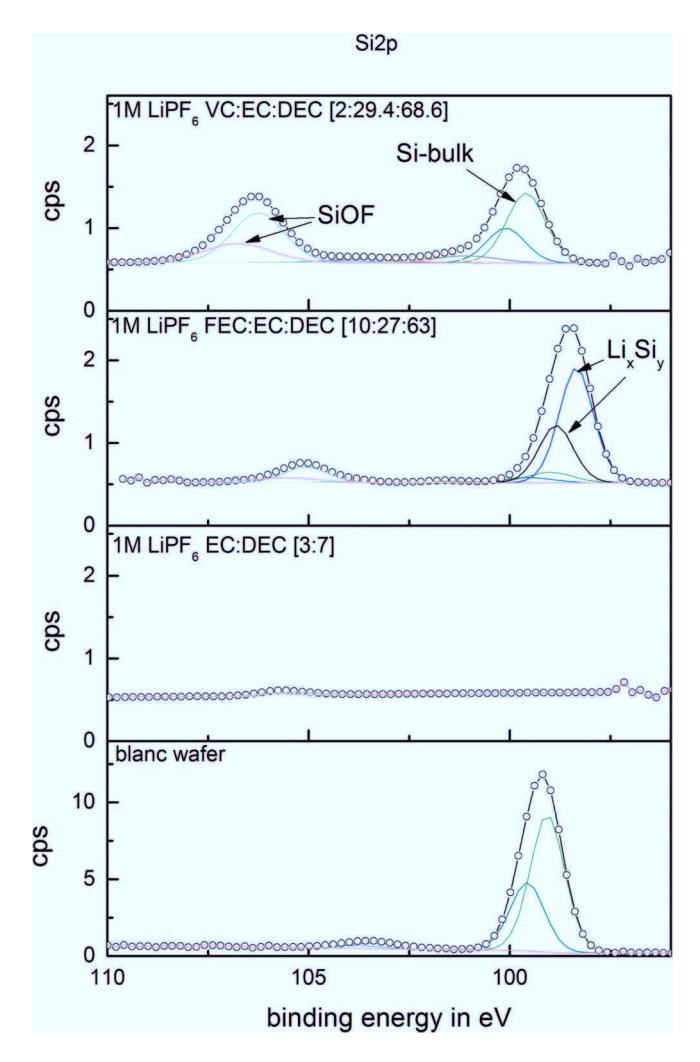


Figure 7. Si 2p XPS spectra of SEI on the Si(100) removed at 0.5 V from 1M LiPF₆, EC:DEC [3:7], 1M LiPF₆, VC:EC:DEC [2:29.4:68.6] and 1M LiPF₆, FEC:EC:DEC [10:27:63].

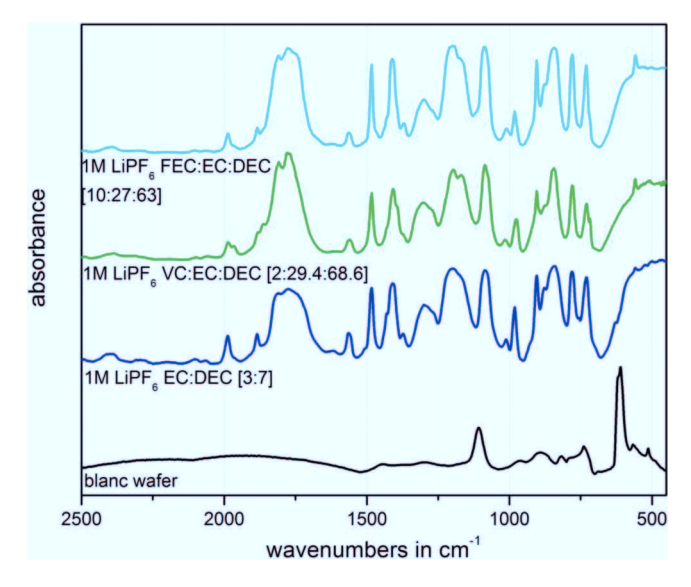


Figure 8. Normalized FTIR spectra of the Si(100) electrode scanned to 0.01 V in 1M LiPF₆ in EC:DEC [3:7], 1M LiPF₆, VC:EC:DEC [2:29.4:68.6] and 1M LiPF₆, FEC:EC:DEC [10:27:63].

ferences in the chemical composition of the SEI layer as compared to the electrode scanned to 0.5 V. The spectra of the Si(100) electrode in the baseline electrolyte recorded at 0.01 V (Figure 8) reveal a slight increase of the Li-F peak at 500 cm⁻¹ and the $\nu_{(P-F)}$ and $\nu_{(P-O-C)}$ modes at 842, 982, 905 and 730 cm⁻¹, respectively. This effect may indicate increased content of inorganic electrolyte decomposition products in the SEI at 0.01 V as compared to 0.5 V (Figure 4).

A closer look at the shape of the broad peak at 1775 cm⁻¹, originating from the symmetric $v_{(C=O)}$ mode, reveals that the right shoulder is less intense in the SEI produced at 0.5 V. Additionally, the (a)symmetric mode $v_{(C=0)}$ at 1300 cm⁻¹ is less pronounced, as well. The lower intensity of these bands, which are attributed to the decomposition products of DEC suggests their lower concentration in the SEI at 0.5 V. This leads to the overall conclusion that at early stages of SEI formation (E>0.5V) the formation mechanism is mainly driven by the decomposition of the organic carbonates, preferably the linear ones, whereas at lower potentials the salt and cyclic carbonates decomposition rates tend to increase significantly.

A similar spectral response is seen in all the three electrolytes, which is a quite unexpected, considering the observed very different electrochemical behavior (Figure 2) and the remarkable differences in the SEI composition at 0.5 V. It appears that the SEI that forms on pristine Si(100) at E>0.5 V undergoes further growth and transformation during silicon alloying with lithium at lower potentials. This produces a fairly consistent SEI on the fully lithiated amorphous Li_xSi at 0.01 V that is fairly independent of the early stages of the SEI layer formation on the pristine Si(100) electrode. Because the Li-Si alloying process is accompanied by a substantial volume expansion, ^{6,8,9} it is almost certain that the early SEI layer formed on the pristine silicon electrode cracks and opens fresh and reactive LixSi surface to the electrolyte, which is immediately followed by reactions with the electrolyte and formation of a "new" SEI layer. Such an electrochemical SEI "self-repair" mechanism at intermetallic negative electrodes such as Sn and Si during continuous cycling has been previously proposed and reported. 41-43 This concept has also been expanded to a thermal SEI repair mechanism, recently. 32,44

On the Si(100) electrode, VC and FEC additives do not influence the formation of the "new" SEI on the lithiated/amorphous LixSi as there is barely a difference visible in the SEI composition at 0.01 V. However, VC and FEC additives have a dramatic effect on the SEI layer behavior on Si(110) and Si(111), which will be subject of the upcoming part II of this study.

Conclusions

The mechanism of early formation stages of the SEI on the single crystal Si(100) electrode at E>0.5 V in organic carbonate-based electrolytes strongly depends on the electrolyte composition. The SEI layer composition, thickness and morphology at 0.5 V is visibly different for the tested electrolytes, indicating the major influence of VC and FEC during early stages of the SEI formation. The SEI formed on Si(100) in the presence of VC and FEC additives is thinner than in the baseline EC:DEC electrolyte and exhibits significant variations in chemical composition. FEC promotes LiF formation, whereas the presence of VC results in a larger fraction of carbon-based organic compounds with various C-O groups and Si-O-F functionalities together with a variety of EC/DEC decomposition products similar to those observed in the SEI formed in the baseline electrolyte. Interestingly, these early differences become negligible once the silicon surface becomes lithiated and turns amorphous. At 0.01 V the chemical composition of the SEI formed on the Si(100) electrode in all the three tested electrolytes with and without additives is very similar and dominated by decomposition products of LiPF₆ and EC.

Acknowledgments

This work was supported by the Assistant Secretary for Energy Efficiency and Renewable Energy, Office of Vehicle Technologies of the U.S. Department of Energy under Contract No. DE-AC0205CH11231, under the Batteries for Advanced Transportation Technologies (BATT) Program. The LBNL Advanced Light Source is supported by the U.S. Department of Energy under Contract No. DE-AC02–05CH11231. The authors also thank Solvay S.A. for providing the FEC additive.

References

- 1. J. M. Tarascon and M. Armand, *Nature*, **414**, 359 (2001).
- 2. T. Placke, V. Siozios, R. Schmitz, S. F. Lux, P. Bieker, C. Colle, H. W. Meyer, S. Passerini, and M. Winter, J Power Sources, 200, 83 (2012).
- 3. R. Wagner, N. Preschitschek, S. Passerini, J. Leker, and M. Winter, J Appl Electrochem, 43, 481 (2013).
- 4. M. N. Obrovac and L. J. Krause, J Electrochem Soc, 154, A103 (2007).
- 5. T. D. Hatchard and J. R. Dahn, J Electrochem Soc, 151, A838 (2004).
- X. H. Hou, S. J. Hu, Q. A. Ru, and Z. W. Zhang, Rare Metal Mat Eng, 39, 2079
- 7. I. Ryu, J. W. Choi, Y. Cui, and W. D. Nix, J Mech Phys Solids, 59, 1717 (2011).
- J. R. Szczech and S. Jin, Energ Environ Sci, 4, 56 (2011).
- C. K. Chan, H. L. Peng, G. Liu, K. McIlwrath, X. F. Zhang, R. A. Huggins, and Y. Cui, Nat Nanotechnol, 3, 31 (2008).
- 10. C. K. Chan, R. Ruffo, S. S. Hong, and Y. Cui, J Power Sources, 189, 1132 (2009).
- 11. R. Ruffo, S. S. Hong, C. K. Chan, R. A. Huggins, and Y. Cui, J Phys Chem C, 113, 11390 (2009).
- 12. W. R. Liu, N. L. Wu, D. T. Shieh, H. C. Wu, M. H. Yang, C. Korepp, J. O. Besenhard, and M. Winter, J Electrochem Soc, 154, A97 (2007).
- 13. M. T. McDowell, S. W. Lee, C. M. Wang, and Y. Cui, Nano Energy, 1, 401 (2012).
- 14. E. Peled, J Electrochem Soc, 126, 2047 (1979).
- 15. D. Aurbach, B. Markovsky, I. Weissman, E. Levi, and Y. Ein-Eli, *Electrochim Acta*, **45**, 67 (1999).
- 16. J. S. Gnanaraj, R. W. Thompson, J. F. DiCarlo, and K. M. Abraham, J Electrochem Soc, 154, A185 (2007).
- 17. D. E. Arreaga-Salas, A. K. Sra, K. Roodenko, Y. J. Chabal, and C. L. Hinkle, J Phys Chem C, 116, 9072 (2012).
- 18. M. Winter, Z Phys Chem, 223, 1395 (2009).
- 19. H. Nakai, T. Kubota, A. Kita, and A. Kawashima, J Electrochem Soc, 158, A798
- 20. N. S. Choi, K. H. Yew, K. Y. Lee, M. Sung, H. Kim, and S. S. Kim, J Power Sources, 161, 1254 (2006).
- 21. L. B. Chen, K. Wang, X. H. Xie, and J. Y. Xie, *J Power Sources*, 174, 538 (2007).
- 22. R. Qiao, I. T. Lucas, A. Karim, J. Syzdek, X. Liu, W. Chen, K. Persson, R. Kostecki, and W. Yang, Advanced Materials Interfaces, 1, n/a (2014).
- 23. I. T. Lucas, J. Syzdek, and R. Kostecki, Electrochem Commun, 13, 1271 (2011).
- 24. K. W. Schroder, H. Celio, L. J. Webb, and K. J. Stevenson, J Phys Chem C, 116, 19737 (2012).
- B. Philippe, R. Dedryvere, J. Allouche, F. Lindgren, M. Gorgoi, H. Rensmo, D. Gonbeau, and K. Edstrom, *Chem Mater*, 24, 1107 (2012).
- 26. S. F. Lux, I. T. Lucas, E. Pollak, S. Passerini, M. Winter, and R. Kostecki, *Electrochem* Commun, 14, 47 (2012).
- 27. W. Kohs, H. J. Santner, F. Hofer, H. Schrottner, J. Doninger, I. Barsukov, H. Buqa, J. H. Albering, K. C. Moller, J. O. Besenhard, and M. Winter, J Power Sources, 119, 528 (2003).
- 28. J. P. Olivier and M. Winter, J Power Sources, 97-8, 151 (2001).
- J. Nawrocki, J Chromatogr A, 779, 29 (1997).
 V. Etacheri, O. Haik, Y. Goffer, G. A. Roberts, I. C. Stefan, R. Fasching, and D. Aurbach, Langmuir, 28, 965 (2012).
- 31. S. Tsubouchi, Y. Domi, T. Doi, M. Ochida, H. Nakagawa, T. Yamanaka, T. Abe, and Z. Ogumi, J Electrochem Soc, 160, A575 (2013).
- 32. I. A. Profatilova, C. Stock, A. Schmitz, S. Passerini, and M. Winter, J Power Sources, 222, 140 (2013).
- 33. B. Philippe, R. Dedryvere, M. Gorgoi, H. Rensmo, D. Gonbeau, and K. Edstrom, Chem Mater, 25, 394 (2013).
- 34. B. Philippe, R. Dedryvere, M. Gorgoi, H. Rensmo, D. Gonbeau, and K. Edstrom, J. Am Chem Soc, 135, 9829 (2013). 35. N. S. Hochgatterer, M. R. Schweiger, S. Koller, P. R. Raimann, T. Wohrle, C. Wurm,
- and M. Winter, Electrochem Solid St. 11, A76 (2008). 36. E. Landemark, C. J. Karlsson, Y. C. Chao, and R. I. G. Uhrberg, Phys Rev Lett, 69,
- 1588 (1992). 37. Y. Nagao, H. Sakaguchi, H. Honda, T. Fukunaga, and T. Esaka, J Electrochem Soc,
- 151, A1572 (2004). 38. M. Miyachi, H. Yamamoto, H. Kawai, T. Ohta, and M. Shirakata, J Electrochem Soc, 152, A2089 (2005).
- 39. Q. Sun, B. Zhang, and Z. W. Fu, Appl Surf Sci, 254, 3774 (2008).
- 40. M. T. McDowell, S. W. Lee, I. Ryu, H. Wu, W. D. Nix, J. W. Choi, and Y. Cui, Nano Lett, 11, 4018 (2011).
- 41. M. Wachtler, J. O. Besenhard, and M. Winter, J Power Sources, 94, 189 (2001).
- 42. H. Bryngelsson, M. Stjerndahl, T. Gustafsson, and K. Edstrom, J Power Sources, 174, 970 (2007)
- 43. M. Wachtler, M. Winter, and J. O. Besenhard, Nano-structured Lithium Storage Alloy Anodes, in The 13th IBA Batteries and Batteries Material Symposium, Marrakesh, Marocco (1999).
- 44. I. A. Profatilova, T. Langer, J. P. Badillo, A. Schmitz, H. Orthner, H. Wiggers, S. Passerini, and M. Winter, J Electrochem Soc, 159, A657 (2012).